석 사 학 위 논 문
Master's Thesis

향상된 시각적 일반화를 통한 모델기반 강화학습 방법론

Model-based Reinforcement Learning with Improved Observational Generalization

2025

박 민 규 (朴 玟 奎 Park, Mingyu)

한 국 과 학 기 술 원

Korea Advanced Institute of Science and Technology

석 사 학 위 논 문

향상된 시각적 일반화를 통한 모델기반 강화학습 방법론

2025

박 민 규

한 국 과 학 기 술 원

전기및전자공학부 (로봇공학 학제전공)

향상된 시각적 일반화를 통한 모델기반 강화학습 방법론

박 민 규

위 논문은 한국과학기술원 석사학위논문으로
학위논문 심사위원회의 심사를 통과하였음

2024년 12월 19일

심사위원장 이 동 환 (인)

심 사 위 원 성 영 철 (인)

심 사 위 원 이 기 민 (인)

Model-based Reinforcement Learning with Improved Observational Generalization

Mingyu Park

Advisor: Donghwan Lee

A dissertation submitted to the faculty of
Korea Advanced Institute of Science and Technology in
partial fulfillment of the requirements for the degree of
Master of Science in Electrical Engineering (Robotics)

Daejeon, Korea
December 19, 2024

Approved by

Donghwan Lee
Professor of Electrical Engineering

The study was conducted in accordance with Code of Research Ethics[1].

[1] Declaration of Ethical Conduct in Research: I, as a graduate student of Korea Advanced Institute of Science and Technology, hereby declare that I have not committed any act that may damage the credibility of my research. This includes, but is not limited to, falsification, thesis written by someone else, distortion of research findings, and plagiarism. I confirm that my thesis contains honest conclusions based on my own careful research under the guidance of my advisor.

MRE 박민규. 향상된 시각적 일반화를 통한 모델기반 강화학습 방법론. 전기및전자공학부 (로봇공학 학제전공) . 2025년. 24+iv 쪽. 지도교수: 이동환. (영문 논문)
Mingyu Park. Model-based Reinforcement Learning with Improved Observational Generalization. School of Electrical Engineering (Robotics Program) . 2025. 24+iv pages. Advisor: Donghwan Lee. (Text in English)

초 록

학습하는 동안 관찰하지 못했던 이미지에 일반화 가능한 강화 학습 (RL) 에이전트를 학습하는 것은 심층 강화학습을 실제 세계에 더 많이 적용할 수 있게 해준다. 이 분야는 이전의 문헌에서 상당한 진전을 관측했지만, 다양한 이미지에 일반화할 수 있고 동시에 샘플 효율을 높일 수 있을지에 대한 의문이 남아있다. 이 연구에서는 우수한 샘플 효율성과 함께 일반화 성능을 촉진하기 위한 새로운 모델 기반 강화학습 방법을 제안한다. 우리의 아이디어는 이미지에 가해진 방해에 관계없이 일관된 표현 (representation) 을 예측하도록 모델을 제한해서 학습하는 것이다. 해당 논문은 다양한 환경과 작업에서 강화학습 에이전트의 일반화 능력을 평가한 광범위한 결과를 제공한다.

핵 심 낱 말 심층 강화학습, 시각적 강화학습, 모델기반 강화학습, 표현 학습, 강화학습에서의 시각적 일반화

Abstract

Learning a generalizable reinforcement learning (RL) agent to the unseen visual image enables further deployments of deep RL into the real world. The field has witnessed significant progress in the prior literature while leaving room for a question: *can RL agent become generalizable to visual input and sample-efficient simultaneously?* In this work, we devise a novel model-based RL method for encouraging generalization performance with superior sample efficiency. Our idea is to constrain the model to predict consistent representation regardless of perturbations. We provide extensive results concerning the generalization ability of RL agents with diverse environments and tasks.

Keywords Deep reinforcement learning, visual reinforcement learning, model-based reinforcement learning, representation learning, and visual generalization in reinforcement learning

Contents

List of Tables

List of Figures

Chapter 1. Introduction

Reinforcement learning (RL) is a branch of machine learning interconnected with the optimal control that trains an agent to maximize expected return by interacting with the environment. While another branch in machine learning, i.e. supervised learning, typically involves collections of correct labels, i.e. optimal actions, to train a decision-making agent that predicts an optimal action, an RL agent can learn which action should be executed based on the value function that predicts future expected return without any supervisions [37]. Furthermore, the RL agent can find an optimal decision rule so-called policy without accurate dynamic information regarding the environment where the agent interacts. This makes RL remarkable in contrast to optimal control which necessitates accurate dynamics for a precise control solution.

Nevertheless, traditional RL exhibits a few limitations regarding more complex decision-making problems. For instance, expensive computing budgets for value and policy learning hamper efficient learning when the state or action space contains high-dimensional information [39], e.g. pixel image state. Recent breakthroughs tackle these problems by combining RL with neural networks to solve diverse decision-making problems [18, 34, 40, 41]. Deep RL becomes more prominent in solving challenging control problems by adopting novel learning techniques [5, 8, 26, 32, 33]. Actually, the agent given eminent representations concerned with decision-making can easily train the accurate value function, leading to superior policy learning. However, one might consider a different but plausible scenario for the agent. What would happen if the agent is given heterogeneous environments between training and evaluation? To give an example, the autonomous driving agent would encounter a road scene similar to the training environment other than the luminosity of view. While humans who acquired expert driving skills can maneuver well regardless of the background brightness, the agent would face severe difficulty in making correct decisions since trained neural networks would fail to predict trustful output when trained on limited data and examined with a similar but unseen view [6].

Alleviating this generalization issue has induced numerous challenges since deep RL often couples policy learning and representation learning. Previous approaches address learning robust representation learning [24, 30, 42, 44, 48], applying stronger data augmentations [13, 14, 20, 23], and stabilizing value function learning[3, 14, 19, 27]. Regarding the data augmentations, enlarging the limited dataset with *weakly* augmented, i.e. random shift, visual data contributes to the significant sample-efficient RL with visual input [23, 45, 46], whereas employing a relatively *strong* augmentation, e.g. random convolution or overlay, improves generalization capability of the agent over unseen image inputs during training.

Interestingly, a common ground shared across these approaches is that they are all model-free RL. Since typical model-based RL exploits samples to learn the policy from the trained model that is responsible for generating extra experiences, the agent of model-based RL manifests poor performance if the model tries to predict future trajectories with unseen input [37]. In contrast, model-free RL usually involves one-step policy improvement with temporal difference learning, where the uncertainty of transition dynamics and expected future return of the given state and action are coupled. However, the nature of coupled value and policy learning essentially decreases the sample efficiency of the RL agent. Furthermore, the stochasticity of the environment or high-dimensional space worsens this problem [47]. Groundbreaking ideas in model-based RL have proven its superior performance and sample efficiency in diverse and challenging continuous control suites in recent years [9, 10, 12, 15, 16]. By learning latent

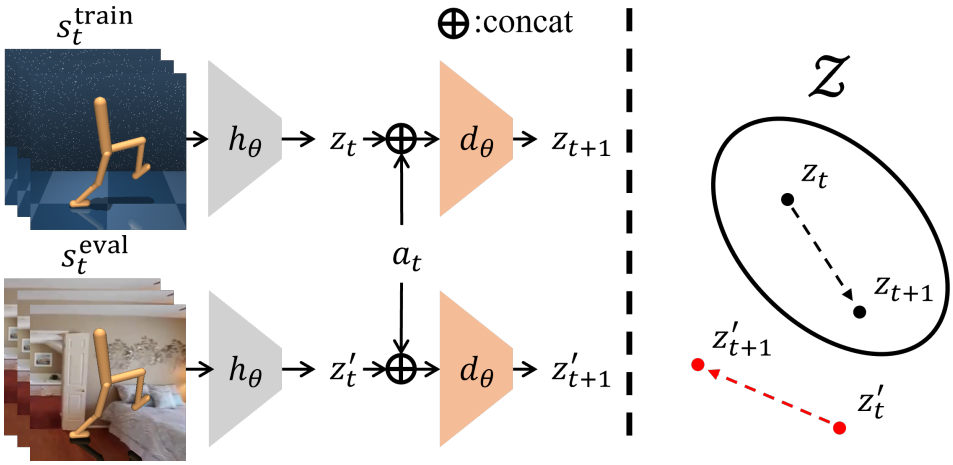

Figure 1.1: **Out-of-distributional representation.** Distribution shift occurs when sampled states between training and evaluation distribution differ. s_t^{train} and s_t^{eval} are example states. h_θ and d_θ are the encoder and transition dynamics, z and z' are extracted representations from in-distributional and out-of-distributional states, respectively. a is an action and $\mathcal{Z}$ is the distribution of z where representations are projected from only the training distribution. Subscript t represents a time step of the environment transition.

transition dynamics model with additional components regarding the model, current model-based RL has validated scalability to higher dimensions and brilliant performance on more complex domains. Thus, one might throw a question in this context, "Can we derive a model-based RL method that enjoys both sample efficiency and better generalization over unseen input by adopting recipes from model-free RL?"

A model-based RL agent with visual input first obtains corresponding representations using a feature extractor, i.e. the encoder, and afterward, rolls out the (latent) transition dynamics model with given representations. Therefore, the encoder that may predict inaccurate representations given unseen image input could be attributed to the collapse of the model-based RL agent since the transition dynamics model would be conditioned on out-of-distributional representations in Figure 1.1. However, we contend that model-based RL can generalize to unseen image input with surpassing sample efficiency based on the idea that projects out-of-distribution image samples to in-distribution representations and generates future representations consistent with the in-distribution samples for the downstream model learning and planning.

In this paper, we propose **M**odel-**B**ased RL with **O**bservational **G**eneralization (MBOG), a model-based RL that empirically demonstrates strong generalization ability over unseen image input without sacrificing sample efficiency by employing recipes from model-free RL. MBOG consists of three key factors for improved performance: (1) applying weak and strong data augmentations to given image input for sample efficiency and generalization, (2) predicting a consistent latent representation simulated by the latent transition dynamics, and (3) regularizing the encoder to extract consistent representations over differently augmented input. We perform extensive experiments to verify our design choice contributes to superior performance on the generalization benchmark [49] across DM-Control [38] and Robosuite [51] benchmarks. By pursuing a comprehensive ablation study, we prove that the proposed design becomes the best fit for solving observational generalization.

Chapter 2. Related Work

2.1 Observational Generalization in Deep RL

Learning a policy that outputs an action maximizing the expected cumulative return under different observation spaces between training and evaluation produces a unique challenge. Observational generalization refers to how the agent trained with visual input maximizes the return during evaluation where the input images from training and evaluation environments are visually different. Prior approaches often incorporate model-free value-based algorithms with representation learning [1, 24, 30, 42, 44, 48], data augmentation [13, 14, 20, 23, 25], and stabilization of value learning [3, 14, 19, 27]. Since jointly learning low-dimensional compact representation from a high-dimensional raw image while capturing optimal behavior from reward signal in an end-to-end manner usually necessitates a large quantity of dataset [31, 35], learning an encoder that can extract helpful information for RL training from data plays a critical role in observational generalization. In this work, we focus on the observational generalization problem in RL similar to prior works. However, we also address the sample efficiency problem during RL training, where prior works have been overlooked. We contend that considering the sample efficiency problem is as significant as the generalization performance since we are given only a limited set of training images according to problem formulation, which exacerbates when a pool of evaluation images increases.

2.2 Model-based Reinforcement Learning

Expanding previous value-based RL methods with the deep neural network has enabled successful adoptions of conventional RL to challenging domains, including a high-dimensional state or continuous action space. However, a prerequisite of a huge bucket of experience replay to learn a well-performing policy becomes a primary bottleneck for RL practitioners [47]. Model-based RL has been introduced as an alternative approach that trains a proxy of the transition model of the environment and exploits the learned model to generate synthetic data for further policy learning [4, 36], allowing the agent to simulate future states and plan the best action to maximize expected return. Since the proxy model is trained via limited collections of the transition, using the ensembles of the trained model [2, 21, 22] alleviates the uncertainty arising from the imperfect model. Learning a world model that simulates future states usually from high-dimensional observations with a latent sequential transition model [7] demonstrates superior sample efficiency and downstream RL performance. Formally, learning a recurrent transition model while reconstructing future images with encoder-decoder structure [9, 10, 12] or combining the planning with model predictive controller without reconstructions [15, 16] proves successful adoption to continuous control of more complicated domains. In this work, we choose TD-MPC [15] as a backbone model-based RL method for observational generalization problems since recent results have shown superior sample efficiency of TD-MPC compared to another state-of-the-art architecture, Dreamer [16]. We provide further discussions concerning model-based RL in Appendix 7.2.1.

Chapter 3. Preliminaries

3.1 Problem Formulation

We design the problem an RL agent tries to solve as the Markov Decision Problem (MDP). MDP is defined as a tuple $\langle \mathcal{S}, \mathcal{A}, \mathcal{T}, r, \gamma \rangle$, where $\mathcal{S}$ is the state space, $\mathcal{A}$ is the action space, $\mathcal{T} : \mathcal{S} \times \mathcal{A} \mapsto \mathcal{S}$ is the transition dynamics probability, and $r : \mathcal{S} \times \mathcal{A} \mapsto \mathbb{R}$ is the reward function. The agent receives not the state directly but the high-dimensional image from the observation space $\mathcal{O}$. Likewise in [14, 46], we define the state s_t as a stack of consequent images for simplicity, i.e. $s_t = \{o_t, o_{t-1}, o_{t_2}, \ldots, o_{t-k+1}\}$ where $s_t \in \mathcal{S}$, $o_t \in \mathcal{O}$, t and k is the time-step and the number of image stacks, respectively. The goal of the agent is to find an optimal policy π^* that maximizes the cumulative expected return $\mathbb{E}_{a_t \sim \pi(\cdot|s_t)} \sum_{t=0}^{\infty} \gamma^t r(s_t, a_t)$ with the discount factor $\gamma \in [0, 1)$.

3.2 Observational Generalization

Following [14, 48, 49], we define the observational generalization problem as a particular problem set where an agent is trained with an MDP $\mathcal{M}$ and evaluated with a set of MDPs $\mathbb{M} = \{\bar{\mathcal{M}}_1, \bar{\mathcal{M}}_2, \ldots, \bar{\mathcal{M}}_n\}$. MDPs in the set share the same tuple with $\mathcal{M}$ other than the perturbed state space $\bar{\mathcal{S}}$ where the state of the perturbed state space $\bar{s} \in \bar{\mathcal{S}}$ is a concatenation of sampled images from the perturbed observation space $\bar{\mathcal{O}}$. The perturbed observation contains partial but essential information about the original observation (e.g., a locomotion agent's body image). During training, an agent receives the state (a stack of images) only from $\mathcal{M} = \langle \mathcal{S}, \mathcal{A}, \mathcal{T}, r, \gamma \rangle$ to find an optimal policy. In contrast, the agent is evaluated with an MDP sampled from $\mathbb{M}$ and given the perturbed state (a stack of perturbed images, $\bar{s}_t = \{\bar{o}_t, \bar{o}_{t-1}, \bar{o}_{t_2}, \ldots, \bar{o}_{t-k+1}\}$) to maximize the expected return, i.e., $\bar{o}_t \in \bar{\mathcal{O}}_i, \bar{\mathcal{M}}_i = \langle \bar{\mathcal{S}}_i, \mathcal{A}, \mathcal{T}, r, \gamma \rangle, \bar{\mathcal{M}}_i \sim \mathbb{M}$. Perturbed images are first sampled from $\mathcal{O}$ and perturbed with a transformation $\nu \sim \mathcal{N}; \nu : \mathcal{O} \times \mathcal{N} \mapsto \mathcal{O}$ that is also sampled from the set of perturbations (e.g., background color change). The goal of an agent is to maximize the expected return during evaluation without any access to the evaluation images during training.

3.3 Temporal Difference learning for MPC

Our method is built upon TD-MPC [15], a model-based RL architecture that combines temporal difference learning [37] for terminal Q value function with the model predictive control (MPC) for planning. TD-MPC is a latent space decoder-free world model that jointly learns parameters of the model: (i) a representation $z = h_\theta(s)$ by encoding a stack of high-dimensional inputs s into a low-dimensional representation z with an encoder h_θ, (ii) a latent dynamics model $z' = d_\theta(z, a)$ that predicts the next latent state z' given current latent state z and action a, (iii) a reward function $\hat{r} = R_\theta(z, a)$ that predicts the one-step reward, (iv) a Q value function $\hat{q} = Q_\theta(z, a)$ that predicts the state-action value function, and (v) a prior policy $\hat{a} \sim \pi_\theta(z)$ that is trained to maximize the Q value function Q_θ and used as a guiding policy for planning. z' and s' are the successor (latent) state while z and s are predecessor (latent) state, respectively.

During online training, the world model is trained via minimizing a weighted loss over the prediction horizon:

$$\mathcal{L}(\theta) = \mathbb{E}_{\Gamma\sim\mathcal{B}}\Bigg[\sum_{i=t}^{t+H}\lambda^{i-t}\Bigg(c_1\Big\|R_\theta(z_t,a_t)-r_t\Big\| + c_2\Big\|d_\theta(z_t,a_t)-h_{\theta^-}(s_{t+1})\Big\| + c_3\Big\|Q_\theta(z_t,a_t)-\mathtt{sg}\big(r_t+\gamma Q_{\theta^-}(\tilde{z}_{t+1},\pi_\theta(\tilde{z}_{t+1}))\big)\Big\|\Bigg)\Bigg], \quad (3.1)$$

where a horizontal trajectory segment $\Gamma = (s_t, a_t, r_t, s_{t+1})_{t:t+H}$ with a horizon H is sampled from the replay buffer $\mathcal{B}$, $\lambda \in \mathbb{R}^+$ is a constant decaying over horizon to weight closer predictions higher, and $c_i \in \mathbb{R}^+, i = 1, 2, 3$ are the coefficients balancing each loss. θ^- stands for exponentially moving average parameters of online parameter θ, $\mathtt{sg}$ is the *stop-grad* operator that prevents the computed gradient from influencing the remaining gradient computations, and $\tilde{z}_{t+1} = h_\theta(s_{t+1}))$ is directly extracted from the online encoder. At each time of the model learning, z_t is encoded from the state s_t first and recursively fed into the latent transition dynamics model d_θ to compute the loss. The prior policy π_θ is trained to maximize the Q value function over horizons only with respect to the policy parameters:

$$\mathcal{L}_\pi(\theta) = \mathbb{E}_{\Gamma\sim\mathcal{B}}\Bigg[\sum_{i=t}^{t+H}\lambda^{i-t}Q_\theta\Big(\mathtt{sg}(z_i), \pi_\theta\big(\mathtt{sg}(z_i)\big)\Big)\Bigg],$$

where the objective is commonly used in model-free actor-critic methods.

During inference (planning), a trained world model is used for the model predictive controller, specifically model predictive path integral (MPPI, [43]). The solution of MPPI can be found by iteratively fitting a time-dependent multivariate Gaussian with diagonal covariance over the action space. The objective of iterative fitting is to maximize the expected return:

$$\hat{R} = \sum_{i=t}^{t+H}\gamma^{i-t}R_\theta(z_t,a_t) + \gamma^H Q_\theta(z_H,a_H),$$

where $z_{t+1} = d_\theta(z_t, a_t)$ and action a_t is sampled from the multivariate normal distribution with the mean u_t^j and diagonal standard deviation σ_t^j at the sampling iteration j and time-step t. The parameters are initialized with zero means and unit standard variance in the action space. Since the reward function is trained to predict the 'instantaneous' reward, i.e., $\hat{r} = R_\theta(z_t, a_t)$, the Q value function allows the agent to fit the optimal action sequence based on 'farsighted' return. We refer to [15] for the additional details.

Chapter 4. Method

In this section, we present MBOG, a model-based RL method that empirically demonstrates strong generalization ability over unseen image input without sacrificing sample efficiency by employing verified recipes from the model-free RL realm. MBOG is built upon TD-MPC has proven strong sample efficiency over continuous control tasks and applies advanced techniques for observational generalization: (1) weak and strong data augmentations to given image input for sample efficiency and generalization, (2) consistent latent representation simulated by the latent transition dynamics and (3) regularization that allows the encoder extract consistent representations over differently augmented input. Our method is compatible with any model-based RL method that learns the latent transition dynamics with a visual feature extractor (the encoder) since we do not constrain any change of the underlying algorithm in principle. In the following, we explain how MBOG tackles the problem by leveraging the core components under the hood.

4.1 Architectural Overview

An overview of MBOG can be found in Figure 4.1. We build our method on top of TD-MPC, a sample-efficient model-based architecture, by fusing the world model learning with data augmentations and representation learning. We employ weak and strong augmentations for latent world model learning by applying weak and strong augmentations to the original image, subsequently. Representations encoded from heterogeneous images are mixed into the latent representation for world model learning (e.g., reward and transition model). Since the world model is trained over the prediction horizon, we regularize the latent dynamics and encoder over the horizon to have consistent representations regardless of an input image. We do not enforce constraints or changes in the model planning procedure.

4.2 Weak and Strong Augmentation

We refer to weak augmentation as employing a relatively minor change in an image (e.g., random shift transformation) and strong augmentation as applying a significant change in the image (e.g., random color convolution). While prior works have shown these augmentations boost the generalization performance and sample efficiency [14, 25, 45], the empirical results are limited to the value-based model-free learning approach. Hence, we propose a novel method for adapting data augmentations into model-based RL. Following prior works, we adopt *random-shift* [45] as weak and *random-overlay* [13] as strong augmentation in this work: *random-shift* augmentation applies a fixed amount of padding to a random direction in *top, bottom, right*, and *left* of the image and *random-overlay* augmentation linearly interpolates between a random image and an original image where the random image is sampled from an unrelated data to the task [50]. Likewise in previous works [13, 14, 48], while one can feed both weakly and strongly augmented images to the encoder in principle, we empirically find that dividing the batch randomly in half and augmenting two sub-batches with different augmentations can produce a similar performance with decreased computing budget. Consider a set of indices $\mathcal{I} = \{1, 2, \ldots, B\}$ where B is the size of the batch. Let the indices of the batch be weakly and strongly augmented as $\mathcal{I}^w$ and $\mathcal{I}^s$,

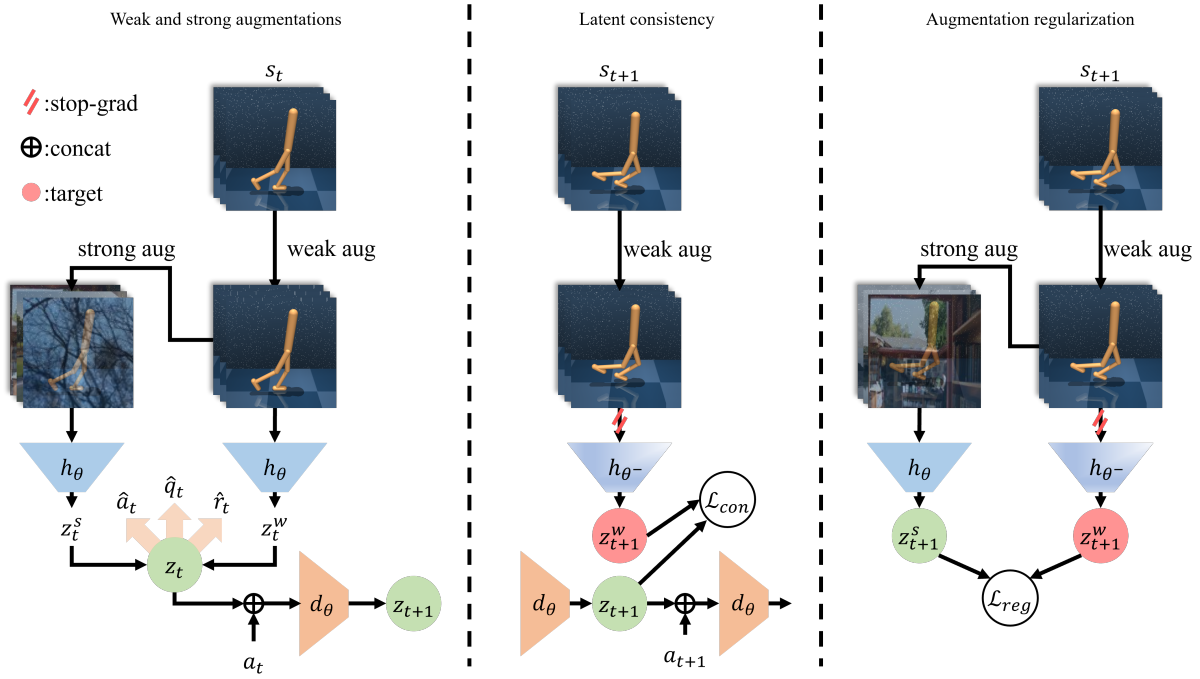

Figure 4.1: **MBOG architecture.** (Left) Weak and strong augmentations are used for observational generalization. (Center)

respectively. Then, the representations from weakly and strongly augmented images at time-step t, i.e., z_t^w and z_t^s, become:

$$z_t^w = h_\theta(\tau^w(s_t)), \quad s_t = \{s_{t,i} : i \in \mathcal{I}^w\},$$
$$z_t^s = h_\theta(\tau^s(s_t^w)), \quad s_t^w = \{s_{t,j}^w : j \in \mathcal{I}^s\},$$

where $z_t = z_t^w \oplus z_t^s$ is the total representation at time-step t where $\oplus$ is element-wise concatenation, τ is an augmentation function given the state s, and $s_{t,n}$ corresponds to the state that is collected by choosing elements in s_t of an index n along the batch dimension. Superscripts w and s state weak and strong augmentation, respectively. $\mathcal{I}^w$ and $\mathcal{I}^s$ are subsets of $\mathcal{I}$ where subsets are complementary and disjoint subsets, i.e., $\mathcal{I}^w \sim \text{Uniform}(1, B), \mathcal{I}^s = \mathcal{I}/\mathcal{I}^w, |\mathcal{I}^w|/|\mathcal{I}^s| = \zeta \in (0, 1)$. Through all experiments, we set the weak and strong augmentation ratio as $\zeta = 0.5$. Since the representation z_t is recursively used for world model learning over the horizon, we apply these augmentations only at time-step t.

4.3 Latent Consistency

While strong data augmentation enables better generalization with unseen visual input, employing strong data augmentation to downstream latent model learning can become problematic. As observed in many prior works [14, 17, 29], noisy and high-variance target values might impede the fast convergence of the Q value function. Since the Q value network is conditioned on the representation in TD-MPC and the representation is encoded from the observation images directly over the horizon, the representation encoded from the strongly augmented image may produce a trivial signal for downstream model learning. However, the field has observed that weak data augmentation often encourages sample-efficient RL in high-dimensional observation space configuration [15, 45, 46]. To enable sample-efficient model learning without sacrificing generalization performance, we constrain the latent representation to have consistency

toward weakly augmented representation z_t^w. After the representation z_t is encoded with weak and strong augmentation, the latent transition dynamics model predicts the successor latent representation z_{t+1} given predecessor z_t and action a_t in the equation 3.1. The parameters of the latent transition dynamics model are updated by solving a regression problem: $\mathcal{L}(\theta; d_\theta) = \text{MSE}(d_\theta(z_t, a_t), z_{t+1})$ where $z_{t+1} = \text{sg}(h_{\theta^-}(s_{t+1}))$. We implement the weak augmentation, i.e., *random-shift*, to the images over the horizon to generate consistent target representation:

$$\begin{aligned}\mathcal{L}_{\text{con}}(\theta; d_\theta) &= \mathbb{E}_{z_{t+1}=d_\theta(z_t,a_t),s_{t+1:t+H}\sim\mathcal{B}}\left[\sum_{i=t+1}^{t+H}\lambda^{i-t}\left(c_2\text{MSE}(d_\theta(z_i,a_i), z_{i+1}^{w,targ})\right)\right] \\ &= \mathbb{E}_{z_{t+1}=d_\theta(z_t,a_t),s_{t+1:t+H}\sim\mathcal{B}}\left[\sum_{i=t+1}^{t+H}\lambda^{i-t}\left(c_2\|d_\theta(z_i,a_i) - \text{sg}(h_{\theta^-}(s_{i+1}^w))\|_2^2\right)\right].\end{aligned}$$

4.4 Regularization over Augmentation

Following the previous steps, the latent transition model and other components of the world model are trained to predict consistent outputs regardless of whether the state in the batch is weakly augmented or strongly augmented. However, the encoder might predict inconsistent representation between training and evaluation images. Although the latent transition model is trained to predict consistent representations over the horizon, the encoder has no constraint to predict a similar representation whether the training or evaluation image is given. Hence, the model should generate reliable synthetic samples regardless of the training or evaluation phase to enable sample-efficient and generalizable model-based RL. To this end, we bring the auxiliary representation learning task to encoder learning during world model training. By regulating the encoder to preserve similar features (e.g., the physical body of the agent) and discarding irrelevant information (e.g., background and luminosity) between the original image and the augmented image, we can obtain consistent representation in both training and evaluation settings. Following [13], we implement the weak and strong augmentation to the state s_t to generate two different views of the original image. Subsequently, we train the encoder h_θ to extract applied strong augmentation in the weakly augmented image by minimizing regularization loss:

$$\begin{aligned}\mathcal{L}_{\text{reg}}(\theta; h_\theta) &= \mathbb{E}_{s_{t:t+H}\sim\mathcal{B}}\left[\sum_{i=t}^{t+H}\lambda^{i-t}\left(\text{MSE}\left(\frac{z_i^s}{\|z_i^s\|_2}, \frac{z_i^{w,targ}}{\|z_i^{w,targ}\|_2}\right)\right)\right] \\ &= \mathbb{E}_{s_{t:t+H}\sim\mathcal{B}}\left[\sum_{i=t}^{t+H}\lambda^{i-t}\left(\left\|\frac{d_\theta(s_i^s)}{\|d_\theta(s_i^s)\|_2} - \text{sg}\left(\frac{h_{\theta^-}(s_i^w)}{\|h_{\theta^-}(s_i^w)\|_2}\right)\right\|_2^2\right)\right]\end{aligned}$$

Chapter 5. Experiments

In this section, we provide experimental results of MBOG on diverse benchmarks. We evaluate the generalization performance and sample efficiency with other baselines. We address the following questions (i) how MBOG compares with other competitive baselines in observational generalization problems, (ii) how our design choice affects the performance of MBOG, and (iii) how MBOG predicts consistent representation over the horizon. We present our implementation details concerning the generalization benchmark and analyze the performance in the following.

5.1 Experiment Setup

In this section, we provide detailed explanations concerning the environmental setup and implementation details for baselines.

Environment. We evaluate MBOG on 6 tasks from the DeepMind control suite (DMC, [38]) and 2 tasks from robosuite [51]: *cartpole_swingup*, *finger_spin*, *walker_walk*, *walker_stand*, *cheetah_run*, and *reacher_easy* in DMC; *Door* and *Lift* in robosuite. We illustrate the tasks and environments in Figure 5.1. We train agents for each task with 1M gradient steps and evaluate the trained agents for 5 seeds. See further details in the environment and task setup in Appendix 7.1.

Baselines. We select state-of-the-art baselines in observational generalization problems to compare MBOG. Specifically, in model-free RL, SVEA [14] stabilizes off-policy Q-learning with data augmentation, SGQN [1] adapts self-supervised learning with attribution map and regularizes Q value learning, SRM [20] applies a spectrum augmentation to increase robustness toward spatial corruption, and PIEG [48] plugs large CNN pretrained with ImageNet for consistent representation. To compare the performance of MBOG with backbone model-based RL, we also evaluate the performance of TD-MPC. Regarding implementation details of baselines, see Appendix 7.1.

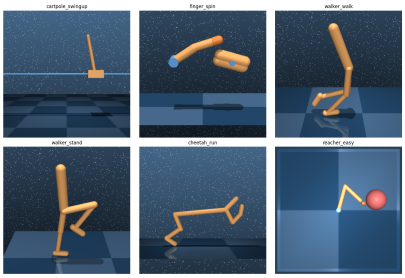

(a) DeepMind Control suite tasks.

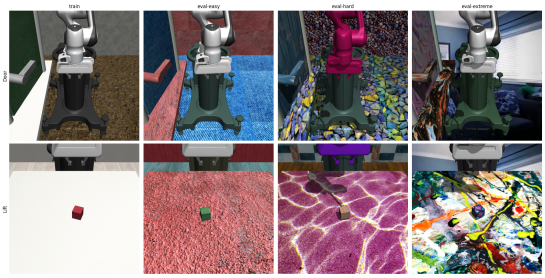

(b) Robosuite tasks.

Figure 5.1: **Environments and tasks.** We consider locomotion and manipulation tasks for observational generalization. We address a set of diverse generalization tasks per each environment.

5.2 Results

5.2.1 How MBOG compares with other competitive baselines in observational generalization problems.

We provide summarized results of performance comparison in Figure 5.2 and Table 5.1. MBOG proves superior sample efficiency over model-free RL in most cases and preserves similar sample efficiency compared to the backbone model-based RL, TD-MPC. In addition, MBOG demonstrates remarkable generalization performance in experiments although it fails to outperform all other baselines. It is worth noting that MBOG outperforms its backbone model, TD-MPC, in generalization performance with a trivial sacrifice of sample efficiency. Considering MBOG does not enforce any algorithmic modifications in model learning and planning with the model, the significant margin of generalization performance supports the validity of the proposed method to alleviate the out-of-distribution shift problem in observational generalization. See full experimental results in Appendix 7.3.

Table 5.1: **Quantitative comparison of generalization performance.** The performance of each algorithm is compared here. Episode return and success rate are reported over tasks in DMC and robosuite, respectively.

Environment	Task	SVEA	SGQN	SRM	PIEG	TD-MPC	MBOG (ours)
DMC	cartpole_swingup	819.67 ±163	635.06±123.50	816.51±182.86	655.53±197.25	678.66±300.24	766.99±206.51
	finger_spin	814.97±305	760.97±307.79	814.93±316.14	780.77±214.09	617.33±356.70	721.62±305.08
	walker_walk	767.19±156	471.38±112.66	886.38±155.28	880.76±165.36	578.05±367.33	814.50±203.11
	walker_stand	947.18±102	876.18±163.26	142.16±29.37	937.51±102.51	667.06±321.88	883.47±143.34
	cheetah_run	435.99±176	226.14±90.50	502.99±155.63	249.32±112.64	379.52±252.26	238.15±95.86
	reacher_easy	801.57±349	217.68±343.67	834.44±321.28	586.87±453.16	461.69±457.92	744.19±367.91
		764.43±275.44	531.24±329.88	666.23±343.59	681.79±329.60	563.72±365.09	694.82±318.48
robosuite	Door	0.0±0.0	0.0±0.0	0.01±0.07	0.92±0.28	0.02±0.14	0.38±0.49
	Lift	0.25±0.43	0.0±0.0	0.27±0.44	0.23±0.42	0.03±0.16	0.18±0.39

5.2.2 How our design choice affects the performance of MBOG.

We address several possible design choices for improving the generalization performance of model-based RL. Toward this objective, we examine the performance of variants of MBOG: dynamic and consistent augmentation, different strong augmentation, and another auxiliary task for representation learning. In the following, we explain the candidates of MBOG and provide a summarized result.

Dynamic and consistent augmentations. We contend that using both weak and strong augmentation contributes to the increased generalization performance of MBOG. Since typical model-based RL predicts future transition samples over the horizon, we suggest a novel model learning scheme with those augmentations. However, it could be unclear whether applying dynamic augmentation over the horizon benefits the generalization performance. Consider the horizontal state $s_{t:t+H}$ with the horizon H during model learning. MBOG augments the states with both weak and strong augmentation over the horizon to constrain latent consistency (Section 4.3) and regularization (Section 4.4). The horizontal states from time-step t to $t+H$ are augmented as:

$$s^w_{t:t+H} = \{\tau^w_k(s_k) : k \in \{t, t+1, \dots, t+H\},$$
$$s^s_{t:t+H} = \{\tau^s_k(s^w_k) : k \in \{t, t+1, \dots, t+H\},$$

where the augmentation function τ can depend on time-step or not. We refer to τ_t as consistent augmentation over the horizon if $\tau_t = \tau_{t+k} \quad \forall k \in [0, H]$ and dynamic otherwise. MBOG adopts dynamic

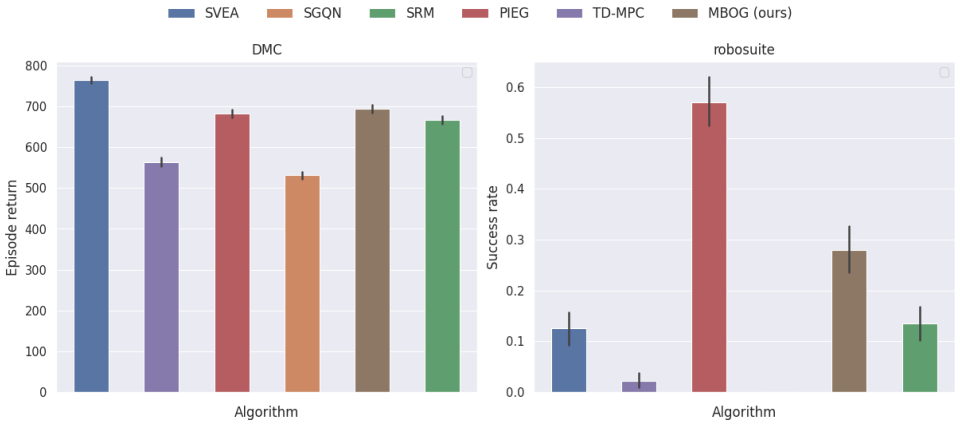

(a) Evaluation results. Episode returns are averaged over 14 evaluation tasks.

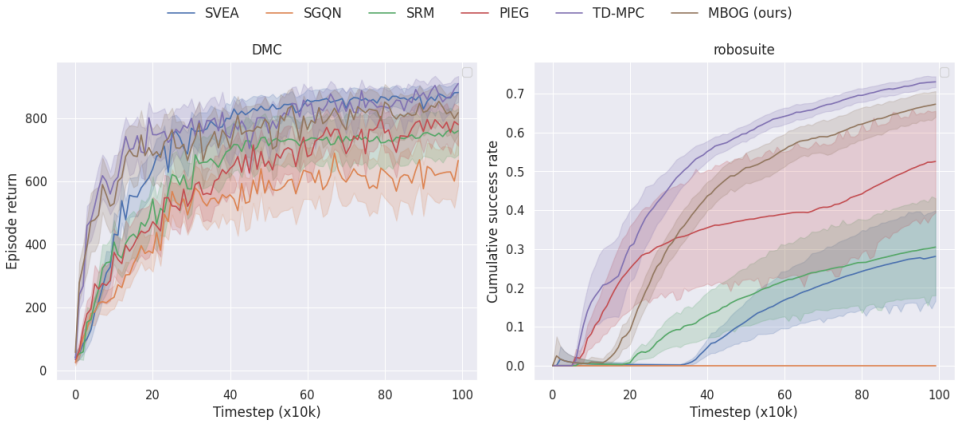

(b) Sample efficiency results. Episode return and cumulative success rate of evaluations during training are reported in DMC and robosuite, respectively. Evaluation during training is averaged over 10 episodes.

Figure 5.2: **Experimental results.** We compare the generalization performance and sample efficiency in diverse experiments. MBOG demonstrates strong sample efficiency compared to previous model-free RL methods and improved generalization ability. TD-MPC also exhibits strong sample efficiency but fails to generalize to unseen images.

augmentation for both weak and strong augmentations, i.e., $\tau_t \neq \tau_{t+k} \quad \forall k \in [0, H]$. We denote MBOG with consistent augmentation as **MBOG_CONST_AUG** later in experiments.

Different strong augmentation. Motivated by prior results [13, 14, 48], we choose *random-overlay* as strong augmentation for observational generalization in model-based RL. However, as proposed in [14, 23, 25], other strong augmentation methods can become candidates for observational generalization in Deep RL. Among potential augmentations, we opt *random-conv* as another strong augmentation method, which exhibits remarkable performance in previous works. Precisely, we refer *random-overlay* and *random-conv* augmentation as:

$$\tau^{s,\text{overlay}}(o) = (1-\delta)o + \delta\tilde{o}$$
$$\tau^{s,\text{conv}}(o) = \text{CONV}(o, w)$$

where $o \in \mathcal{O} = \mathbb{R}^{B\times C\times H\times W}$ is the augmented images with the batch size B, channel C, height H, and

width W, respectively. δ is a linear interpolation coefficient, $\tilde{o} \sim \mathcal{D}$ is an overlaying image sampled from a dataset unrelated to the task. We set the default value of δ as 0.5. CONV stands for 2-dimensional convolution operation over the batch dimension and $w \in \mathbb{R}^{N \times C_k \times H_k \times W_k} : w \sim \mathcal{N}(0, 1)$ is the convolution filter randomly initialized with the normal distribution and kernel number N, channel C_k, height H_k, and width W_k, respectively. We implement the same strong augmentation over the channel dimension to obtain the state $s_t = \{o_t, o_{t-1}, \cdots, o_{t-k+1}\}$. While MBOG chooses *random-overlay* as strong augmentation, we denote **MBOG_CONV** as MBOG replaced with *random-conv*.

Different strong augmentation. Learning proper representation for vision-based RL plays a critical role in sample efficiency and generalization performance. Prior literature [1, 17, 24, 30, 48] has explored the field by leveraging popular representation learning techniques in computer vision. As in Section 4.4, we intend the encoder to predict robust representation regardless of distracting components (e.g., background image). Hence, we consider two variants of auxiliary representation learning task: *SODA* [13] and *CURL* [24]:

$$\mathcal{L}_{CURL}(\theta, h_\theta) = \mathbb{E}_{s_{t:t+H} \sim \mathcal{B}} \left[\sum_{i=t+1}^{t+H} \lambda^{i-t} \left(\log \frac{\exp q^T W k_+}{\exp q^T W k_+ + \sum_{j=0}^{B} \exp q^T W k_j} \right) \right],$$

where $q = h_\theta(\tau^w(s_t))$ is the anchor, $k = h_{\theta^-}(\tau^w(s_t))$ is the key, and W is the weight kernel for bilinear product. We implement different *weak* augmentation to generate anchor and positive samples. We denote **MBOG_CURL** as MBOG replacing the regularization loss (i.e., $\mathcal{L}_{\text{reg}} = \mathcal{L}_{\text{SODA}}$) with $\mathcal{L}_{\text{CURL}}$.

Aggreagated results. We provide the total experimental results in Figure 5.3. We compare MBOG with *MBOG_CONST_AUG*, *MBOG_CONV*, and *MBOG_CURL* in *finger_spin* and *walker_walk* tasks. MBOG proves superior sample efficiency and generalization performance compared to other options while validating that the proposed method is outstanding. See further experimental details regarding this comparison in Appendix 7.3.

Figure 5.3: **Experiments comparing design choices.** We have considered several methodologies for building generalizable model-based RL. Among the potential choices, MBOG proves its superiority in experiments.

5.2.3 How MBOG predicts consistent representation over the horizon.

To reduce the prediction error of the world model, we proposed a novel approach that constrains the world model learning with data augmentation and representation learning. The idea below the method is

that it is important not only to constrain the consistent representation recursively predicted by the latent transition model but also to predict robust representation regardless of distracting factors. Hence, we experiment to validate the idea that MBOG would satisfy the conditions for observational generalization while TD-MPC fails. The conditions for consistent representation are (1) The latent representations predicted by the transition model should be aligned with the future latent representations from the encoder and (2) The encoder should predict consistent representations between the original and unseen images. We collect the horizontal replay transitions by rolling out the trained model and feeding the same input (i.e., $(s_t, a_t, s_{t+1})_{t:t+H}$) to MBOG and TD-MPC to predict the representations. Since the representation has more than two dimensions, we visualize the result with UMAP [28] in Figure 5.4, a popular manifold learning method to extract two-dimensional coordinates from representations.

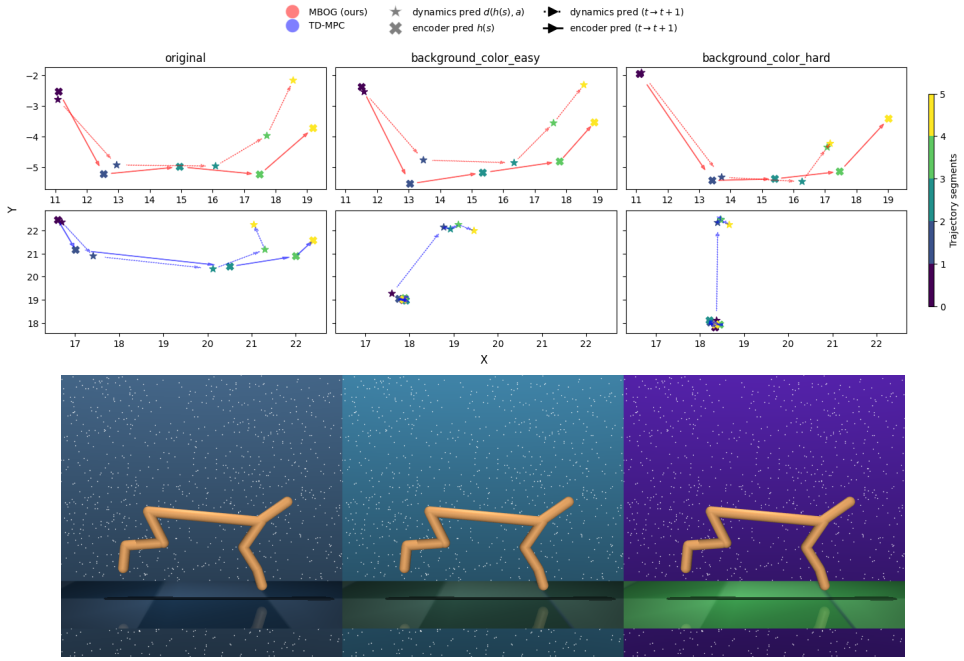

Figure 5.4: **Visualization of embeddings.** We visualize the embedding vectors using UMAP. (Top) MBOG shows consistent representation over the horizon and types of evaluation. (Bottom) Illustration of types used for extracting representation over different types of generalization.

While TD-MPC struggles to output consistent representation over the horizon, MBOG demonstrates aligned representation between the latent dynamics prediction $\hat{z}_{t+1} = d_\theta(z_t, a_t)$ and the encoder prediction $z_{t+1} = h_\theta(s_{t+1})$. Furthermore, MBOG manifests similar representation prediction ability regardless of generalization types (i.e., between *original*, *background_color_easy*, and *background_color_hard*) while TD-MPC predicts far-away representation from the original (trained) distribution, demolishing the accuracy of latent transition dynamics model. See additional details in Appendix 7.3.

5.3 Discussion and Future Work

MBOG achieves superior generalization ability to unseen image inputs with similar sample efficiency to TDMPC. By constraining the world model learning with data augmentation and representation learning, MBOG can achieve a remarkable generalization performance without losing the superior sample efficiency of model-based RL. However, there are a few setbacks for model-based RL to overcome in observational

generalization. First, the performance gain of MBOG is still below the state-of-the-art model-free RL. While it is notable that MBOG improves the generalization ability over TD-MPC, previous works (e.g., SVEA [14]) achieve better generalization performance than MBOG in experiments. Second, the computing cost of planning is still high. Since the model is used not only for gathering samples during training but also for planning an optimal action during evaluation, reducing the computing cost raised by the model rollout should be the next step to adopting model-based RL into observational generalization in RL. We hope that future work will resolve the problems and push the boundaries of model-based RL in observational generalization.

Chapter 6. Conclusion

We have proposed MBOG, a model-based RL that empirically demonstrates strong generalization ability over unseen image input without sacrificing sample efficiency by employing recipes from model-free RL. By constraining the world model to predict consistent representation with data augmentation and representation learning, MBOG successfully solves the observational generalization problem. We provide extensive results for comparing the performance between model-free and model-based RL. We believe that further transitions from the model-based RL field into the observation generalization realm enable exciting future works.

Bibliography

[1] D. Bertoin, A. Zouitine, M. Zouitine, and E. Rachelson. Look where you look! saliency-guided q-networks for generalization in visual reinforcement learning. *Advances in Neural Information Processing Systems*, 35:30693–30706, 2022.

[2] J. Buckman, D. Hafner, G. Tucker, E. Brevdo, and H. Lee. Sample-efficient reinforcement learning with stochastic ensemble value expansion. *Advances in neural information processing systems*, 31, 2018.

[3] E. Cetin, P. J. Ball, S. Roberts, and O. Celiktutan. Stabilizing off-policy deep reinforcement learning from pixels. *arXiv preprint arXiv:2207.00986*, 2022.

[4] M. Deisenroth and C. E. Rasmussen. Pilco: A model-based and data-efficient approach to policy search. In *Proceedings of the 28th International Conference on machine learning (ICML-11)*, pages 465–472, 2011.

[5] S. Fujimoto, H. Hoof, and D. Meger. Addressing function approximation error in actor-critic methods. In *International conference on machine learning*, pages 1587–1596. PMLR, 2018.

[6] I. Goodfellow. Deep learning, 2016.

[7] D. Ha and J. Schmidhuber. World models. *arXiv preprint arXiv:1803.10122*, 2018.

[8] T. Haarnoja, A. Zhou, P. Abbeel, and S. Levine. Soft actor-critic: Off-policy maximum entropy deep reinforcement learning with a stochastic actor. In *International conference on machine learning*, pages 1861–1870. PMLR, 2018.

[9] D. Hafner, T. Lillicrap, J. Ba, and M. Norouzi. Dream to control: Learning behaviors by latent imagination. *arXiv preprint arXiv:1912.01603*, 2019.

[10] D. Hafner, T. Lillicrap, I. Fischer, R. Villegas, D. Ha, H. Lee, and J. Davidson. Learning latent dynamics for planning from pixels. In *International conference on machine learning*, pages 2555–2565. PMLR, 2019.

[11] D. Hafner, T. Lillicrap, M. Norouzi, and J. Ba. Mastering atari with discrete world models. *arXiv preprint arXiv:2010.02193*, 2020.

[12] D. Hafner, J. Pasukonis, J. Ba, and T. Lillicrap. Mastering diverse domains through world models. *arXiv preprint arXiv:2301.04104*, 2023.

[13] N. Hansen and X. Wang. Generalization in reinforcement learning by soft data augmentation. In *2021 IEEE International Conference on Robotics and Automation (ICRA)*, pages 13611–13617. IEEE, 2021.

[14] N. Hansen, H. Su, and X. Wang. Stabilizing deep q-learning with convnets and vision transformers under data augmentation. *Advances in neural information processing systems*, 34:3680–3693, 2021.

[15] N. Hansen, X. Wang, and H. Su. Temporal difference learning for model predictive control. *arXiv preprint arXiv:2203.04955*, 2022.

[16] N. Hansen, H. Su, and X. Wang. Td-mpc2: Scalable, robust world models for continuous control. *arXiv preprint arXiv:2310.16828*, 2023.

[17] K. He, H. Fan, Y. Wu, S. Xie, and R. Girshick. Momentum contrast for unsupervised visual representation learning. In *Proceedings of the IEEE/CVF conference on computer vision and pattern recognition*, pages 9729–9738, 2020.

[18] M. Hessel, J. Modayil, H. Van Hasselt, T. Schaul, G. Ostrovski, W. Dabney, D. Horgan, B. Piot, M. Azar, and D. Silver. Rainbow: Combining improvements in deep reinforcement learning. In *Proceedings of the AAAI conference on artificial intelligence*, volume 32, 2018.

[19] S. Huang, Y. Sun, J. Hu, S. Guo, H. Chen, Y. Chang, L. Sun, and B. Yang. Learning generalizable agents via saliency-guided features decorrelation. *Advances in Neural Information Processing Systems*, 36, 2024.

[20] Y. Huang, P. Peng, Y. Zhao, G. Chen, and Y. Tian. Spectrum random masking for generalization in image-based reinforcement learning. *Advances in Neural Information Processing Systems*, 35: 20393–20406, 2022.

[21] M. Janner, J. Fu, M. Zhang, and S. Levine. When to trust your model: Model-based policy optimization. *Advances in neural information processing systems*, 32, 2019.

[22] T. Kurutach, I. Clavera, Y. Duan, A. Tamar, and P. Abbeel. Model-ensemble trust-region policy optimization. *arXiv preprint arXiv:1802.10592*, 2018.

[23] M. Laskin, K. Lee, A. Stooke, L. Pinto, P. Abbeel, and A. Srinivas. Reinforcement learning with augmented data. *Advances in neural information processing systems*, 33:19884–19895, 2020.

[24] M. Laskin, A. Srinivas, and P. Abbeel. Curl: Contrastive unsupervised representations for reinforcement learning. In *International conference on machine learning*, pages 5639–5650. PMLR, 2020.

[25] K. Lee, K. Lee, J. Shin, and H. Lee. Network randomization: A simple technique for generalization in deep reinforcement learning. *arXiv preprint arXiv:1910.05396*, 2019.

[26] T. Lillicrap. Continuous control with deep reinforcement learning. *arXiv preprint arXiv:1509.02971*, 2015.

[27] S. Liu, Z. Chen, Y. Liu, Y. Wang, D. Yang, Z. Zhao, Z. Zhou, X. Yi, W. Li, W. Zhang, et al. Improving generalization in visual reinforcement learning via conflict-aware gradient agreement augmentation. In *Proceedings of the IEEE/CVF International Conference on Computer Vision*, pages 23436–23446, 2023.

[28] L. McInnes, J. Healy, and J. Melville. Umap: Uniform manifold approximation and projection for dimension reduction. *arXiv preprint arXiv:1802.03426*, 2018.

[29] V. Mnih. Playing atari with deep reinforcement learning. *arXiv preprint arXiv:1312.5602*, 2013.

[30] S. Nair, A. Rajeswaran, V. Kumar, C. Finn, and A. Gupta. R3m: A universal visual representation for robot manipulation. *arXiv preprint arXiv:2203.12601*, 2022.

[31] J. Pari, N. M. Shafiullah, S. P. Arunachalam, and L. Pinto. The surprising effectiveness of representation learning for visual imitation. *arXiv preprint arXiv:2112.01511*, 2021.

[32] J. Schulman. Trust region policy optimization. *arXiv preprint arXiv:1502.05477*, 2015.

[33] J. Schulman, F. Wolski, P. Dhariwal, A. Radford, and O. Klimov. Proximal policy optimization algorithms. *arXiv preprint arXiv:1707.06347*, 2017.

[34] D. Silver, A. Huang, C. J. Maddison, A. Guez, L. Sifre, G. Van Den Driessche, J. Schrittwieser, I. Antonoglou, V. Panneershelvam, M. Lanctot, et al. Mastering the game of go with deep neural networks and tree search. *nature*, 529(7587):484–489, 2016.

[35] A. Stooke, K. Lee, P. Abbeel, and M. Laskin. Decoupling representation learning from reinforcement learning. In *International conference on machine learning*, pages 9870–9879. PMLR, 2021.

[36] R. S. Sutton. Dyna, an integrated architecture for learning, planning, and reacting. *ACM Sigart Bulletin*, 2(4):160–163, 1991.

[37] R. S. Sutton. Reinforcement learning: An introduction. *A Bradford Book*, 2018.

[38] Y. Tassa, Y. Doron, A. Muldal, T. Erez, Y. Li, D. d. L. Casas, D. Budden, A. Abdolmaleki, J. Merel, A. Lefrancq, et al. Deepmind control suite. *arXiv preprint arXiv:1801.00690*, 2018.

[39] C. R. Taylor. Dynamic programming and the curses of dimensionality. In *Applications of dynamic programming to agricultural decision problems*, pages 1–10. CRC Press, 2019.

[40] H. Van Hasselt, A. Guez, and D. Silver. Deep reinforcement learning with double q-learning. In *Proceedings of the AAAI conference on artificial intelligence*, volume 30, 2016.

[41] Z. Wang, T. Schaul, M. Hessel, H. Hasselt, M. Lanctot, and N. Freitas. Dueling network architectures for deep reinforcement learning. In *International conference on machine learning*, pages 1995–2003. PMLR, 2016.

[42] Z. Wang, Y. Ze, Y. Sun, Z. Yuan, and H. Xu. Generalizable visual reinforcement learning with segment anything model. *arXiv preprint arXiv:2312.17116*, 2023.

[43] G. Williams, A. Aldrich, and E. Theodorou. Model predictive path integral control using covariance variable importance sampling. *arXiv preprint arXiv:1509.01149*, 2015.

[44] S. Yang, Y. Ze, and H. Xu. Movie: Visual model-based policy adaptation for view generalization. *Advances in Neural Information Processing Systems*, 36, 2024.

[45] D. Yarats, R. Fergus, A. Lazaric, and L. Pinto. Mastering visual continuous control: Improved data-augmented reinforcement learning. *arXiv preprint arXiv:2107.09645*, 2021.

[46] D. Yarats, I. Kostrikov, and R. Fergus. Image augmentation is all you need: Regularizing deep reinforcement learning from pixels. In *International conference on learning representations*, 2021.

[47] D. Yarats, A. Zhang, I. Kostrikov, B. Amos, J. Pineau, and R. Fergus. Improving sample efficiency in model-free reinforcement learning from images. In *Proceedings of the aaai conference on artificial intelligence*, volume 35, pages 10674–10681, 2021.

[48] Z. Yuan, Z. Xue, B. Yuan, X. Wang, Y. Wu, Y. Gao, and H. Xu. Pre-trained image encoder for generalizable visual reinforcement learning. *Advances in Neural Information Processing Systems*, 35:13022–13037, 2022.

[49] Z. Yuan, S. Yang, P. Hua, C. Chang, K. Hu, and H. Xu. Rl-vigen: A reinforcement learning benchmark for visual generalization. *Advances in Neural Information Processing Systems*, 36, 2024.

[50] B. Zhou, A. Lapedriza, A. Khosla, A. Oliva, and A. Torralba. Places: A 10 million image database for scene recognition. *IEEE transactions on pattern analysis and machine intelligence*, 40(6):1452–1464, 2017.

[51] Y. Zhu, J. Wong, A. Mandlekar, R. Martín-Martín, A. Joshi, S. Nasiriany, and Y. Zhu. robosuite: A modular simulation framework and benchmark for robot learning. *arXiv preprint arXiv:2009.12293*, 2020.

Chapter 7. Appendix

7.1 Implementation Details

In this section, we describe the implementation details concerning the environments and baselines. We bring overall source code from RL-ViGen [49][1]. We thank the authors of RL-ViGen for providing comprehensive source code.

Environment. We consider 14 evaluation types in DMC and 4 evaluation types in robosuite. In DMC, we consider the *type* and *difficulty* of the evaluation: *background_color*, *cam_pos*, *background_video*, *light_position*, *light_color*, *moving_light*, and *object_color* for types; *easy* and *hard* for difficulty. In robosuite, we consider 3 types of evaluation *eval-easy*, *eval-hard*, and *eval-extreme*, which is predefined by [49].

Figure 7.1: **Evaluation set in DMC.**

[1] https://github.com/gemcollector/RL-ViGen

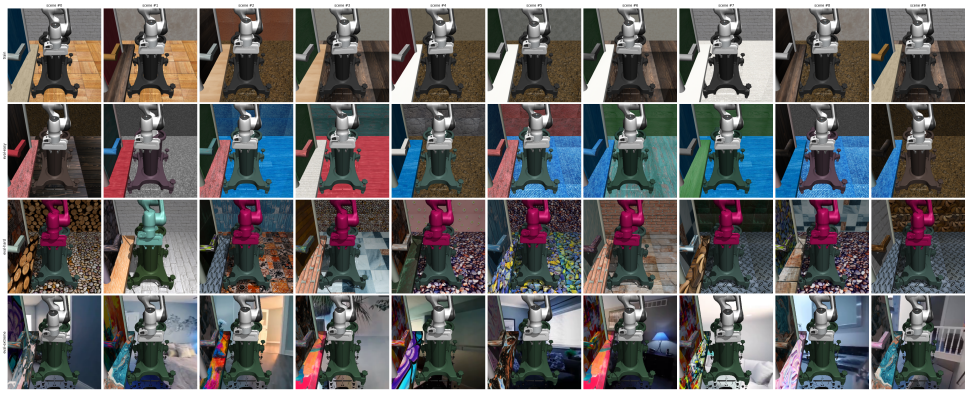

Figure 7.2: **Evaluation set in robosuite.**

Baselines. We consider 4 baselines for model-free (SVEA [14], SGQN [1], SRM [20], and PIEG [48]) and TD-MPC([15]) for model-based algorithms for comparison. We conduct experiments under the RL-ViGen benchmark since the source code of 4 model-free baselines is implemented straightforwardly. We adapt the source code of TD-MPC from the original repository[2]. We use the same hyperparameter over experiments per each algorithm following previous works.

7.2 Discussions

7.2.1 Model-based RL

Our main contribution to this paper is to present a model-based RL method that empirically demonstrates strong generalization ability without sacrificing sample efficiency. We have compared two state-of-the-art model-based RL backbone algorithms, TD-MPC [15], and DreamerV2 [11], which exhibit strong sample efficiency over diverse continuous control problems. The reason for not choosing update-to-date versions of each model-based RL method is to reproduce the proper results with the original paper (e.g., TD-MPC compared its performance with DreamerV2, which was the most recent version of the Dreamer series) and to benefit the architecture itself without further technical considerations since the most recent versions of each algorithm, TD-MPC2 [16], and DreamerV3 [12], contain extensive techniques for improving performance. We provide reproduced experiments to validate that TD-MPC would exhibit better sample efficiency than DreamerV2 in Figure 7.3. Since our purpose is to achieve sample-efficient RL for observational generalization, we choose TD-MPC as our backbone model-based RL algorithm.

[2] https://github.com/nicklashansen/tdmpc

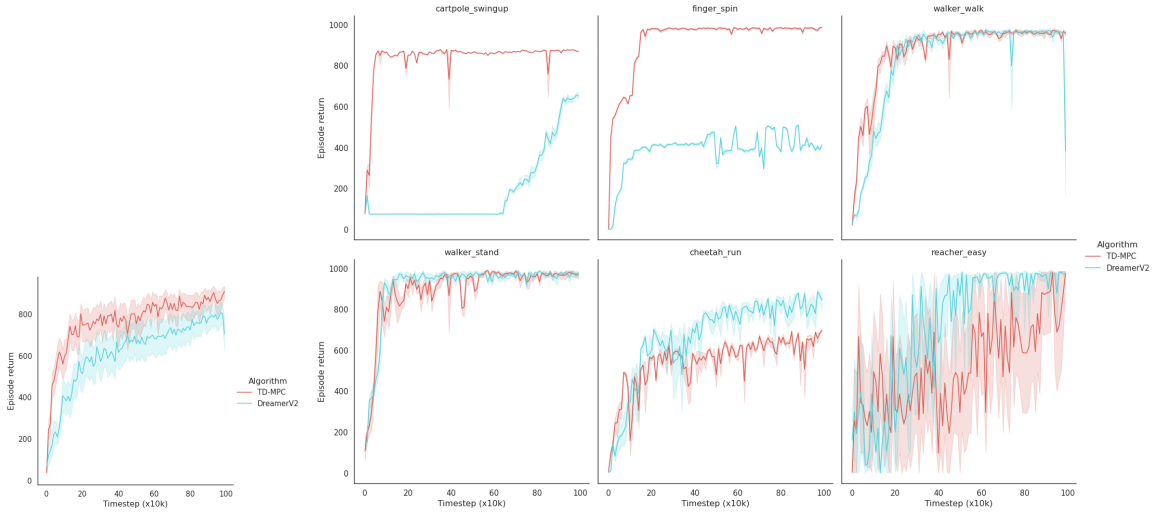

(a) Total comparison result.

(b) Comparison over tasks in the DeepMind Control suite.

Figure 7.3: **Comparison of sample efficiency between model-based RL methods.** TD-MPC demonstrates superior sample efficiency over DreamerV2 in 6 tasks in the DeepMind Control suite benchmark.

7.3 Additional Results

We provide full results for extensive experiments here.

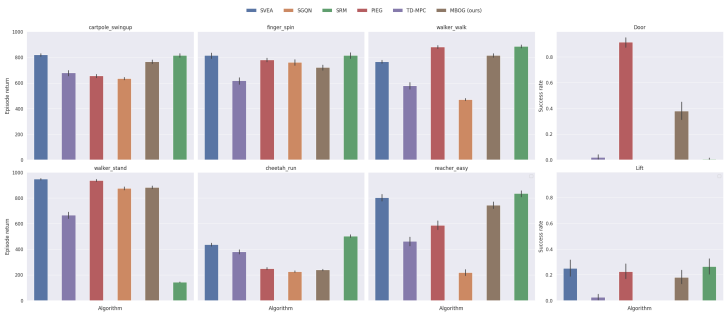

(a) Evaluation results over environments and tasks.

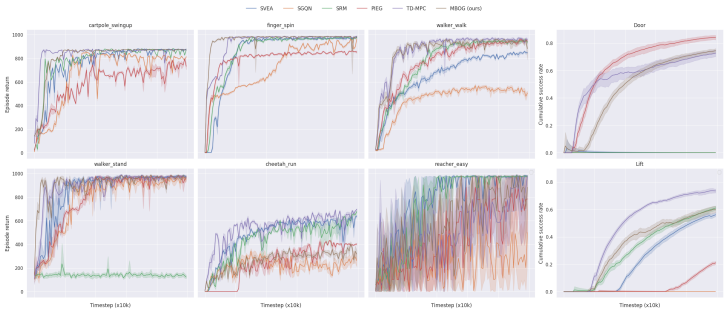

(b) Sample efficiency over environments and tasks.

Figure 7.4: **Additional experimental results over tasks.** Episode returns and cumulative success rates over tasks are reported in DMC and robosuite, respectively.

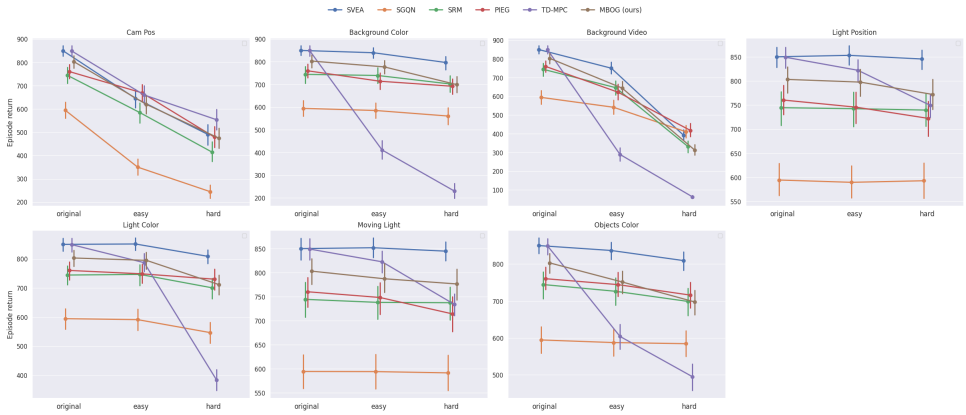

(a) Episode return over evaluation types.

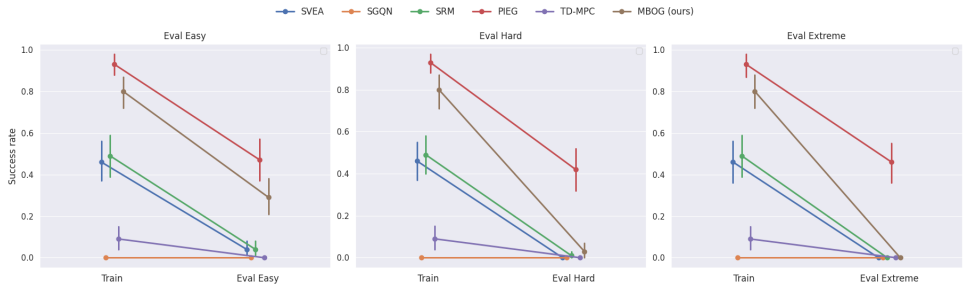

(b) Success rate over evaluation types.

Figure 7.5: **Evaluation results over evaluation types.** We compare the performance of baselines in a total of 14 types. Generalizable RL methods show a monotonic decrease between original and generalization types (e.g., original-easy-hard).

We provide full experimental results of comparing possible options over environments.

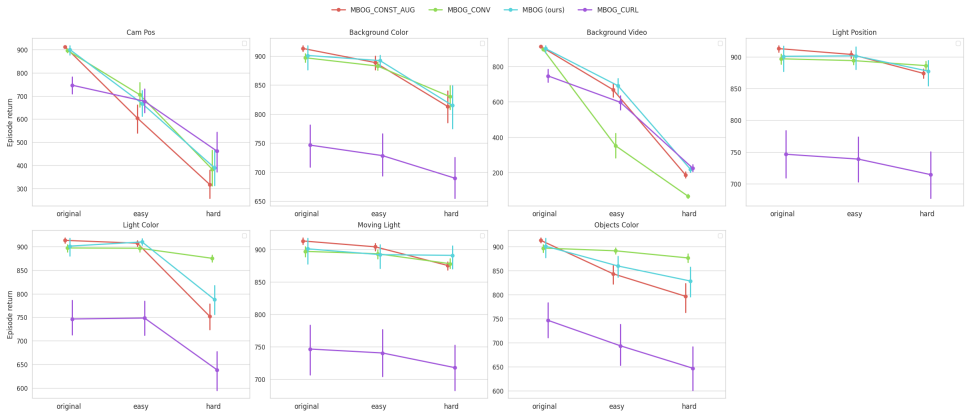

Figure 7.6: **Evaluation results over evaluation types for options.** We compare the performance of our design choices in a total of 14 types. MBOG shows a monotonic decrease between original and generalization types (e.g., original-easy-hard) compared to other options.

We illustrate how the strong augmentation would be applied to the original image.

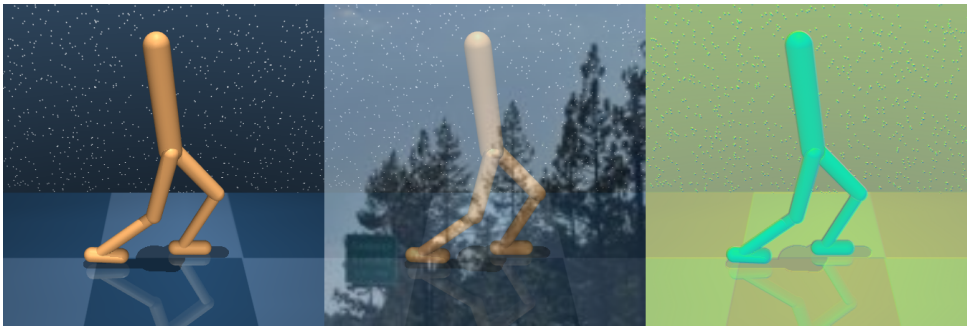

Figure 7.7: **Example images comparing strong augmentations.** Illustrations of how the image is augmented in *walker_walk* task. (Left) Original image, (Center) *random-overlay* augmentation, (Right) *random-conv* augmentation.

We provide full plots for embedding experiments. We choose *cheetah_run* for embedding experiments.

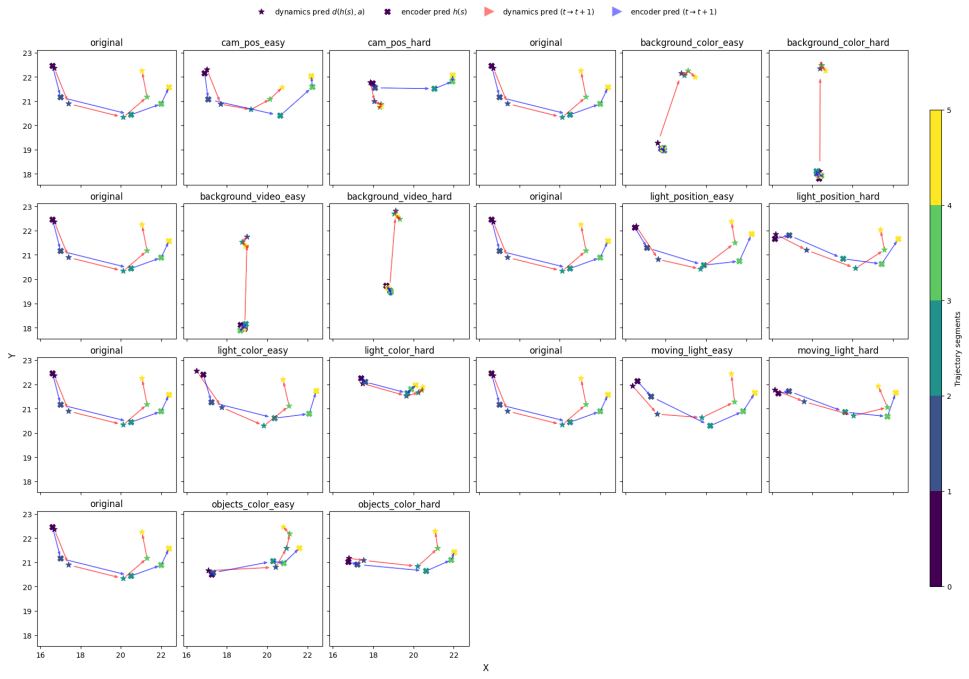

Figure 7.8: **Visualization of embeddings from TD-MPC.**

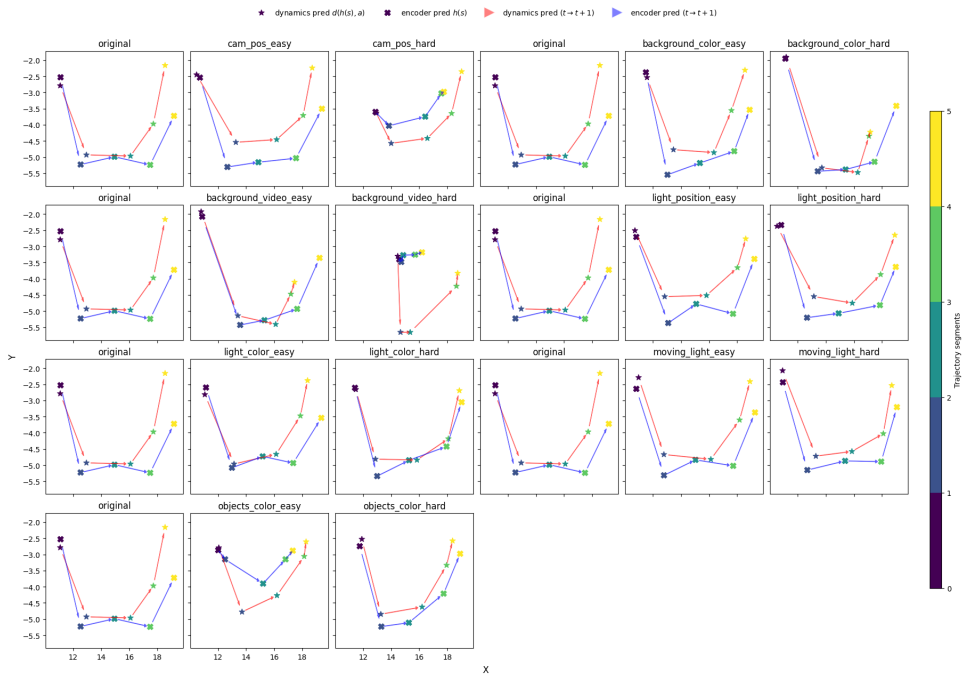

Figure 7.9: **Visualization of embeddings from MBOG.**

Figure 7.10: **Visualization of types for an embedding experiment.** We plot horizontal images used for extracting representations over the generalization types.